Assessment of Runoff Sensitivity in the Upper Indus Basin to Interannual Climate Variability and Potential Change Using MODIS Satellite Data Products

Authors: Forsythe, Nathan, Kilsby, Chris G., Fowler, Hayley J., and Archer, David R.

Source: Mountain Research and Development, 32(1) : 16-29

Published By: International Mountain Society

URL: https://doi.org/10.1659/MRD-JOURNAL-D-11-00027.1

Mountain Research and Development (MRD)
An international, peer-reviewed open access journal
published by the International Mountain Society (IMS)
www.mrd-journal.org

MountainResearch
Systems knowledge

Assessment of Runoff Sensitivity in the Upper Indus Basin to Interannual Climate Variability and Potential Change Using MODIS Satellite Data Products

Nathan Forsythe[1], Chris G. Kilsby[1], Hayley J. Fowler[1], and David R. Archer[2]*

** Corresponding author: nathan.forsythe@newcastle.ac.uk*

[1] Newcastle University, School of Civil Engineering & Geosciences, Water Resources Research Group, Newcastle-upon-Tyne, United Kingdom

[2] JBA Consulting, South Barn, Broughton Hall, Skipton, North Yorks BD23 3AE, United Kingdom

The Upper Indus Basin (UIB) covers an area of more than 200,000 km^2 and has an elevation range from below 1000 to over 8000 m above sea level. Its water resources underpin Pakistan's food security and energy supply. Vertical and horizontal variations in key climate variables govern the runoff contributions of the UIB's various elevation zones and subcatchments. Remote sensing climatic data products from NASA's Moderate Resolution Imaging Spectrometer (MODIS) instrument platform provide an opportunity to develop a spatial characterization of the climatology of remote and rugged regions such as the UIB. Specifically, snow-covered area (SCA) and land surface temperature (LST) have been shown to provide good analogues, respectively, for precipitation and air temperature. As such, SCA and LST quantify regional variations in mass and energy inputs to runoff generation processes. Although the 10-year (2000–2010) MODIS observational record is not adequate to evaluate long-term trends, it does provide a consistent depiction of annual cycles and a preliminary assessment of interannual variability. This study presents a summary of the period means and interannual variability found in remotely sensed SCA and LST products for the UIB. It then provides an update of locally observed recent climate trends for the 1962 to 2007 period. Nonparametric trend tests are applied both to the local observations and to remote sensing records to assess patterns in recent variability. The climatic noise (intense variability) of the past decade, however, renders conclusions on nascent trends in SCA and LST premature. Finally, runoff sensitivity to temperature change—spatially applied as summer (JJA) nighttime 0°C LST isotherm migration—is assessed for a range of potential scenarios. Results indicate that changes in mean summer (JJA) runoff could range from −30 to +35% or more, depending on whether recent locally observed changes continue or scenarios derived from current regional climate model (RCM) simulations unfold.

Keywords: *Indus; MODIS; snow; LST; climatology; interannual variability.*

Peer-reviewed: *September 2011* ***Accepted:*** *October 2011*

Introduction

The Indus River is the lifeblood of Pakistan, principally in supporting irrigated agriculture and hence food security (Archer et al 2010). Hydropower also underpins energy security (Tarbela Dam supplies approximately 20% of the national electricity demand). In addressing the need for improved knowledge management to support enhanced water productivity, Karki et al (2011) note, "Disruption in the hydrological regime can have serious impacts on people's lives in the basin …" Thus, as Karki et al point out, key priorities are (1) improved understanding of hydroclimatic variability and potential and (2) expanded use of available remote sensing data sets.

Recent studies have attempted to address the macroscale issues of future water availability in major Asian river basins through the use of remote sensing. For example, Immerzeel et al (2010) assessed precipitation using Tropical Rainfall Measurement Mission (TRMM) (Huffman 2007). However, TRMM data, derived from infrared and passive microwave-based rainfall estimation algorithms, show deficiencies when measuring orographic precipitation (Dinku 2008). Field observations of high-elevation precipitation in the Upper Indus Basin (UIB) show significant orographic dependency (Hewitt 2011). For example, Forsythe et al (2011) note that for tributary catchments with seasonal snowmelt-type hydrological regimes with minimal glacial contribution, TRMM precipitation estimates account for only ~40 to 60% of observed river discharge (expressed as runoff depth in mm). Thus, care is needed when extrapolating conclusions from these products to variations in glacial

 http://dx.doi.org/10.1659/MRD-JOURNAL-D-11-00027.1

FIGURE 1 The Upper Indus Basin in Pakistan showing topography and measurement networks. (Map by N. Forsythe)

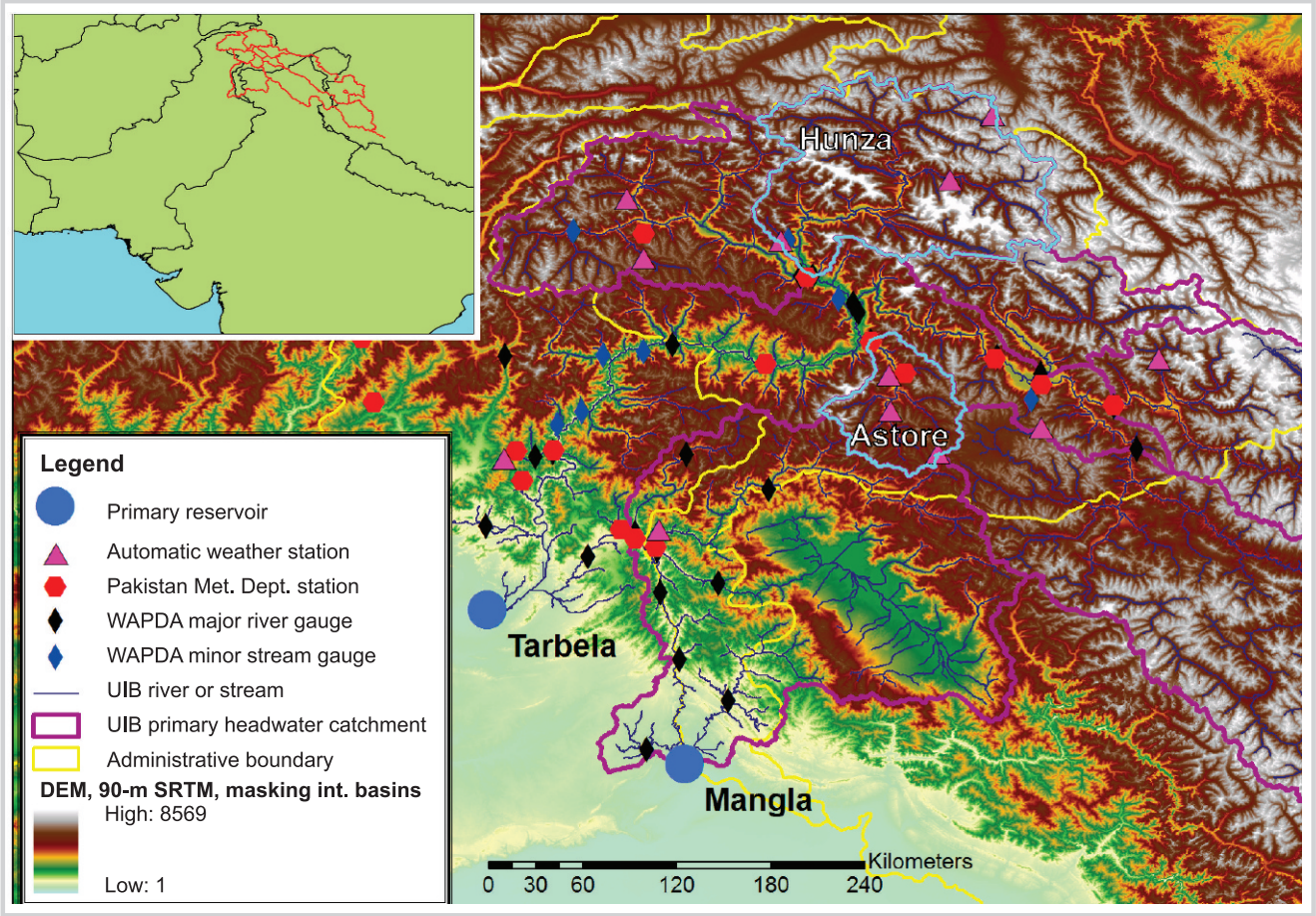

mass balance and future trends in water availability. The approach presented here treats remotely sensed data products as quantitative indicators of catchment conditions rather than as absolute measures.

Study area and data limitations

Locally observed data from the Pakistan Meteorological Department (PMD) and the Pakistan Water and Power Development Authority (WAPDA) are of crucial value in understanding regional climate. Ground-based data have been shown to be representative of large-scale hydrological variability (Archer and Fowler 2008) but do not adequately define altitudinal variations. Local observations can also be used to validate remotely sensed data, which provide good spatial coverage, albeit with limited historical record lengths. Useful spatial data products for catchments dominated by runoff from snowmelt and glacial melt are estimates of snow-covered area (SCA) and land surface temperature (LST) as available from the Moderate Resolution Imaging Spectrometer (MODIS) instrument. SCA and LST data products are validated here by (1) direct comparison to point observations or estimates derived from them and (2) correlations of variability in spatially aggregated parameters to variability in point-based analogues.

Large-scale hydrology of the UIB

The scale of vertical range and variation within the UIB has few analogues elsewhere in the world. Elevation ranges from below 1000 m, where the river emerges on the plains at the 2 major controlling reservoirs of Tarbela and Mangla (Figure 1), to several mountain peaks above 8000 m. This vertical range, combined with the magnitude of the annual temperature cycle and the accumulation and ablation of precipitation as snow and ice, defines the hydrology of the basin.

Runoff in the UIB is primarily composed of meltwater from ephemeral snow and perennial glacial masses, with a smaller contribution from direct winter or monsoon rainfall from foothill catchments (Archer 2003). The relative contributions from these 3 sources of runoff (direct rainfall, seasonal snow, and perennial ice) give rise

http://dx.doi.org/10.1659/MRD-JOURNAL-D-11-00027.1

FIGURE 2 Hypsometry of the NW UIB and monthly extrapolated 0°C isotherm elevations.

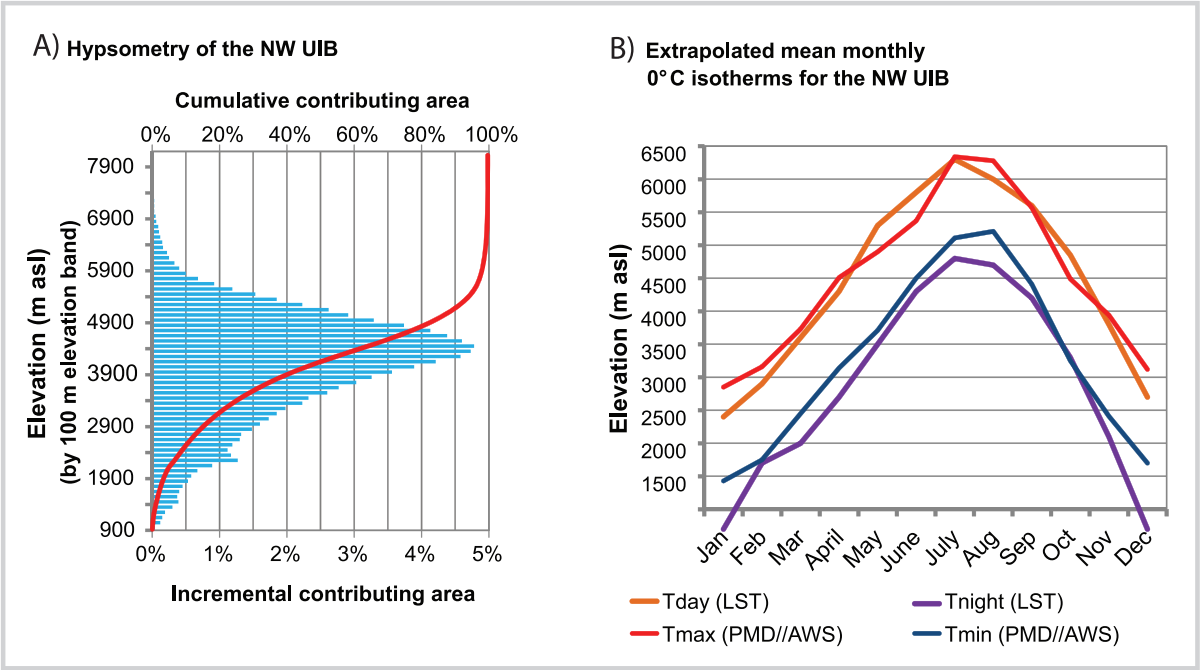

to 3 distinct hydrological regimes (Archer 2003). While the contribution of precipitation inputs to snowpack mass balance is immediately obvious, the energy controls on meltwater generation processes are less intuitive. Daily minimum temperatures are a key element, as nighttime refreezing disrupts meltwater processes (Bengtsson 1982). A key metric for assessing thermal constraints to runoff generation is thus the fraction of the catchment where monthly mean nighttime temperatures remain above 0°C, defined here as the "continuous melt area" (CMA). The particular hypsometry of the UIB—the high percentage of surface area in the elevation range where the average daily minimum temperature (Tmin) 0°C isotherm fluctuates during the summer—means that this parameter is highly sensitive to incremental temperature anomalies. This is illustrated in Figure 2.

The contrasting controls of temperature and precipitation on the timing and magnitude of the annual hydrological cycle are shown here for the River Astore, a catchment dominated by melt of seasonal snow (Figure 3A, B), and for the River Hunza, where runoff is mainly derived from glaciers and perennial snow (Figure 3C, D). For the River Astore (Figure 3A), melt runoff is initiated while the catchment is still warming and recedes before it cools, once the available snowpack has been exhausted. For the River Hunza (Figure 3C), meltwater generation is correlated with CMA (Tmin > 0°C): flows increase in late spring and remain high until temperatures fall in early autumn. Comparing the interannual variations between the 2 catchments, the years of maximum and minimum flow volume do not match because the controlling parameters (precipitation and temperature) are largely independent at this timescale.

Note that CMA (Tmin > 0°C) in Figure 3 is determined by linear extrapolation of the estimated lapse rate to calculate the elevation of the 0°C isotherm. This elevation is then cross-referenced against the catchment hypsometry (ie the vertical distribution of catchment area) to identify the percentage of the catchment below the 0°C isotherm.

Previous studies (Archer 2003, Archer and Fowler 2008, Forsythe et al 2011) have shown significant linear correlations between gauged river flows and observed climate in the UIB, notably, concurrent temperature or preceding season precipitation. These relationships differ between the 3 identified regimes. Examples of such relationships are shown by Forsythe et al (2011) for the Astore catchment and for the high-level Hunza catchment (their Figure 7; repeated here as Figure 3A, D). Strong relationships are found between the relative anomalies of summer (June to August) discharge and winter (October to March) precipitation for the Astore catchment, and summer discharge and concurrent temperature at Gilgit shown as CMA (Tmin > 0°C) for the Hunza catchment. These relationships indicate the sensitivity of UIB hydrology to both present climate variability and developing trends.

Methodology

Archer and Fowler (2008) used measurements from long-record meteorological stations to identify relationships between local climate observations and regional

http://dx.doi.org/10.1659/MRD-JOURNAL-D-11-00027.1

FIGURE 3 Typical catchment regime responses to climate variability. (A and B) Astore catchment; (C and D) Hunza catchment; (A and C) response in timing of flows; (B and D) response in magnitude of flows. (Panels B and D are from Forsythe et al 2011, their Figure 7)

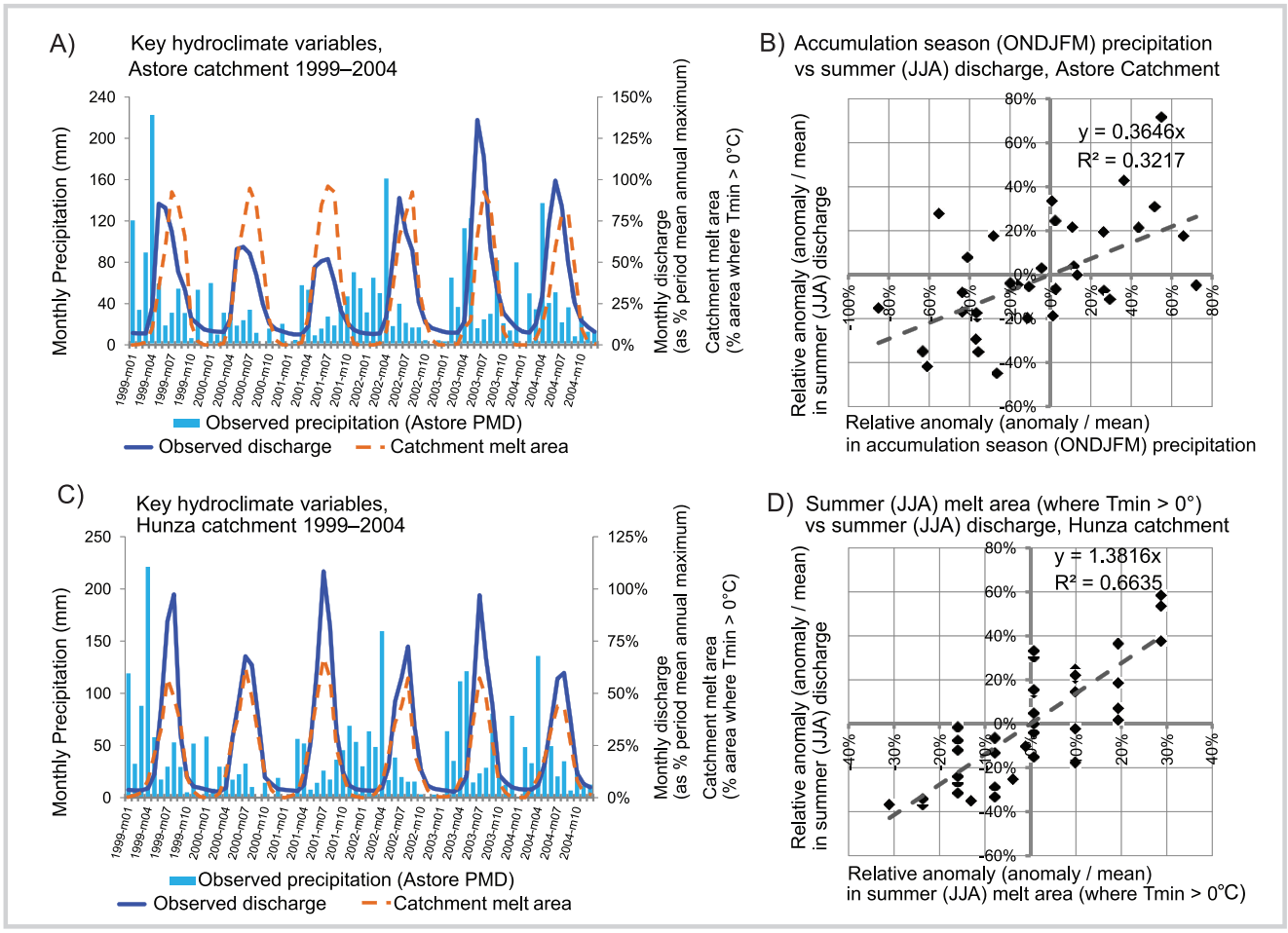

hydrological responses in the UIB. Forsythe et al (2011) utilized remotely sensed spatial data products to extend this methodology. In place of air temperature and precipitation, LST and SCA were used as indicators of inputs of energy and mass to meltwater generation processes contributing the bulk of runoff in the UIB. We first summarize the results of their study before detailing updated recent trends in observed climate variables, using parametric and nonparametric trend testing, and then test their correlation with trends in LST and SCA.

The MODIS SCA and LST data products

The data products are derived from radiometric measurements made by the MODIS instrument flown aboard NASA's Terra platform. The algorithms for both SCA and LST depend upon "clear sky conditions." This means that for a given pixel, in order to determine the snow cover state or calculate its LST, it must be cloud-free. For this reason, data used here are from consecutive 8-day temporal aggregates assimilating the available observations during the period. Given the cloud climatology of the Upper Indus, most satellite scenes are partially cloud covered. In general, pixels over valley bottoms will be cloud-free more often than pixels covering mountain tops. Thus, the count of observations contributing to 8-day aggregates will most often be greater for low elevation zones than higher ones.

SCA, as 8-day aggregates of maximum extent—note that maximum snow extent indicates that a pixel observed as both snow covered and snow free by daily observations during the 8-day period is classified as snow covered—at a 500-m horizontal resolution (product MOD10A2 [Hall et al 2001]), is used as an analogue for precipitation observed at local meteorological stations. Day and nighttime LST, in the form of 8-day aggregates (mean of available observations) at a 1-km horizontal resolution (product MOD11A2 [Wan 2008]), are used as analogues of locally observed average daily maximum (Tmax) and minimum (Tmin) 2-m air temperature. The MODIS data products are available from early 2000 to the present.

Forsythe et al (2011) assessed the LST and SCA data products with respect to air temperature observations at

http://dx.doi.org/10.1659/MRD-JOURNAL-D-11-00027.1

FIGURE 4 Validation of MODIS spatial data products using local air temperature observations.

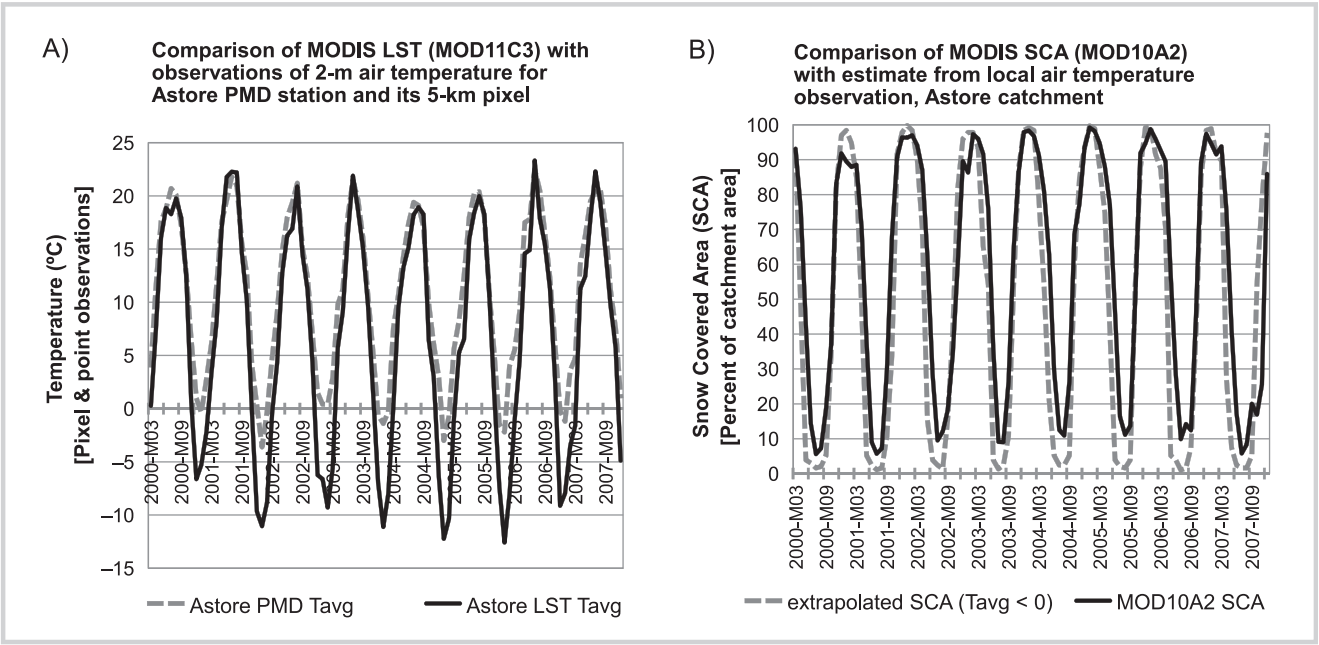

Astore for 2000 to 2007. A time series of average LST was extracted for the pixel overlying Astore and compared to Astore average temperature (Tavg). SCA was assessed by estimating snow cover as the fraction of the study area where mean daily air temperature is below freezing (0°C, as in Jain 2008). This was then extrapolated in the same way as for CMA, using the hypsometric data for the Astore catchment. Both LST and SCA were found to track well with respective local estimates (Figure 4; Figure 3 in Forsythe et al 2011) in timing and interannual variability, especially for annual maxima. However, there was a clear and consistent divergence in annual minima for both data products. Forsythe et al (2011) explained this divergence using snow cover dynamics. During the winter, snow cover is nearly complete and the snow pack surface temperature becomes appreciably colder than the overlying air temperature through the accumulation of thermal inertia, also known as "cold content" (Bras 1990). During the spring and summer, as the snow pack warms and then melts and SCA diminishes, the LST and air temperature converge. The divergence between remotely sensed SCA and the simple estimate based on local air temperature appears during the ablation phase when the reduction in SCA (from snowmelt) lags behind the air temperature.

Analysis of relationships between spatial data and point observations

To demonstrate that SCA and LST are equivalent counterparts to locally observed precipitation and temperature, specific indicators were chosen within the SCA and LST data products as the closest spatial approximation of the local indicators used to characterize UIB hydrology (see "Large-scale hydrology of the UIB" above).

At the individual pixel-scale, SCA is an effectively discrete measure of the surface state—ie snow covered (1) or snow-free (0). Therefore, an analogue for catchment winter precipitation mass input is not immediately obvious. For the accumulated winter precipitation (ONDJFM) indicator, March SCA was selected, as it is usually close to the annual maxima and represents the catchment snow state at the transition from accumulation to ablation phase. Fortunately, while not a perfect analogue for air temperature, LST tracks reliably enough to be used as derived. The time-varying behavior of these indicators, aggregated as spatial means for each catchment, was tested against local observations from three long-running stations using "standardized anomalies." The standard anomaly time series were calculated individually for each indicator, both local and spatial, by subtracting the period means from each observation and then dividing by the period standard deviation.

The results of the correlation analyses (Pearson's "*r*," 2-tailed significance) are shown in Tables S1 and S2 (*Supplemental data*; http://dx.doi.org/10.1659/MRD-JOURNAL-D-11-00027.S1) for the catchments in Figure 5. Due to the steep vertical precipitation gradients reported in the UIB (Hewitt 2011), March SCA was tested against both accumulated winter precipitation depth and the seasonal total number of wet days. As precipitation is highly variable in space and time, correlation would be expected to be limited. Statistical significance is also challenging given the short common observation record (and annual time-step

FIGURE 5 Primary gauged UIB headwater tributary basins and available local meteorological stations. Primary gauged catchments: 1, Hunza river to Dainyor bridge; 2, Shigar river to Shigar town; 3, Gilgit river to Gilgit town; 4, Astore river to Doyian; 5, Shyok river to Yogo; 6, high Indus to Kharmong. Note that the NW UIB analysis unit (0) is shown with hash marks and is comprised of catchments 1 through 4 plus the Indus main channel gorge from Besham Qila upstream to the gauging stations at Kharmong and Yogo; the Upper Indus to Besham comprises the NW UIB plus catchments 5 and 6. (Map by N. Forsythe. This figure also appears in Forsythe et al 2011, as their Figure 1.)

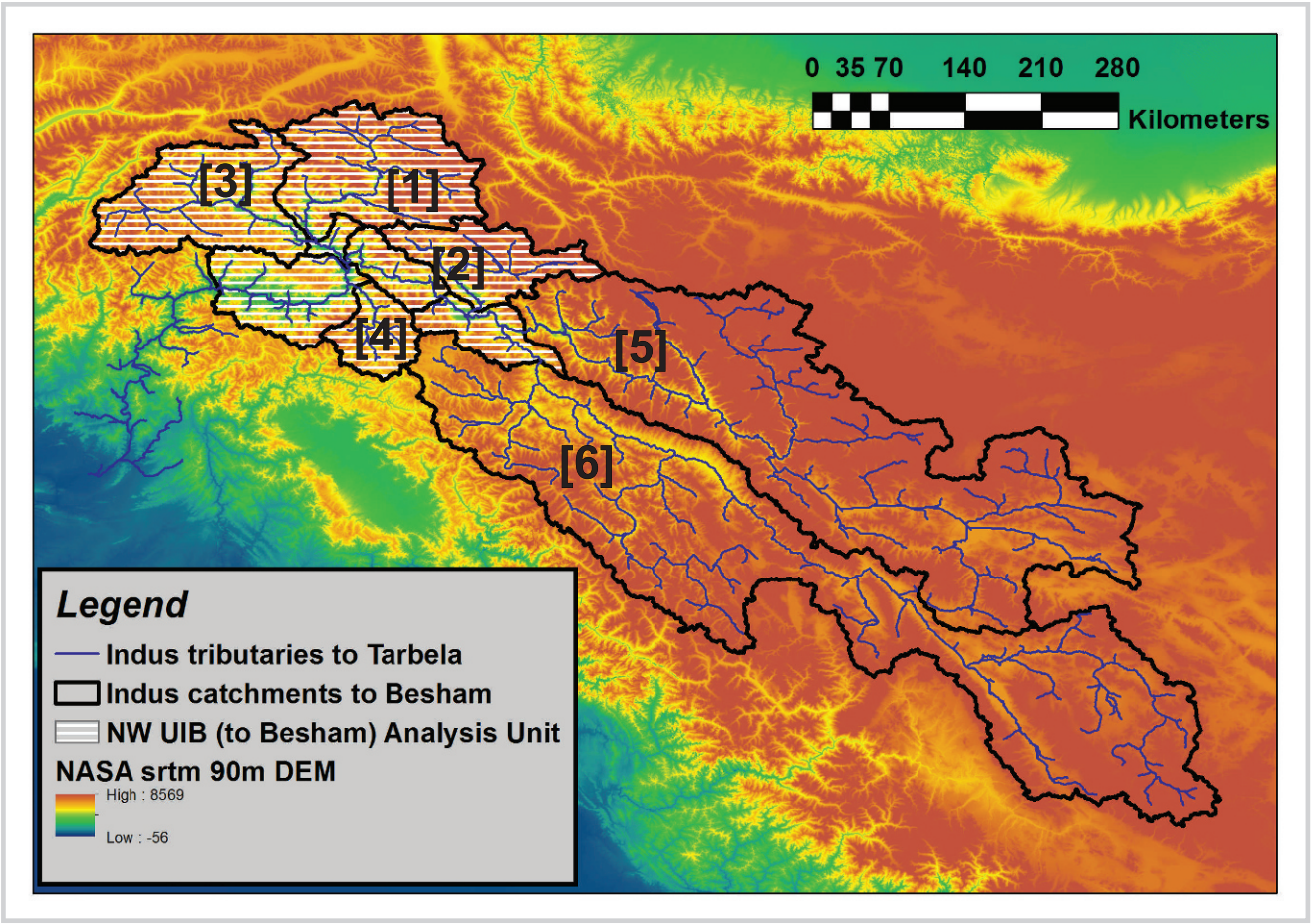

comparison). However, strong correlations at statistically significant levels are found in several cases. These strong correlations demonstrate the March SCA is a valid analogue for the accumulated winter precipitation (ONDJFM) observed at the local meteorological stations.

For the LST to air temperature correlations, the greater sample size (required length divided by the shorter monthly time-step) yields more statistically significant relationships. The higher correlation coefficients for daytime/Tmax comparisons over nighttime/Tmin counterparts are also expected, as the same pattern is found when testing correlation between local stations. The primary finding here is that correlations for both "Tmax versus Tday" and "Tmin versus Tnight" are frequently greater than 0.5, thus demonstrating the validity of LST—even spatially aggregated over large tributary catchments—as an indicator for local observations of air temperature.

Correlation analysis was used to further test the coherence of the spatial data products within each catchment. Physically, snow cover and surface temperature are linked not only by their concurrent states but also by cumulative antecedent precipitation and persistent temperature anomalies. Even so, the simple comparison of concurrent anomalies in the correlation analysis results shown in Table S3 (*Supplemental data*; http://dx.doi.org/10.1659/MRD-JOURNAL-D-11-00027.S1) demonstrates that UIB subcatchments are quite responsive as spatial units. An example of these relationships, for the Gilgit catchment, is graphically represented in Figure 6.

Given that variations in temperature will often be due to large-scale systems taking more than a single day to pass through the study area, strong correlations would be expected between daytime and nighttime LST. Strong negative correlations between both LST measures and SCA would also be expected, given that SCA will decrease during warm conditions and persist or increase during cooler weather. The coherence of these results further strengthens the case for the use of these spatial data products as hydroclimatic indicators.

Determination of hydrological regime types and runoff sensitivities from SCA and LST

A core concern for improving the resilience of infrastructure and resource management systems to cope

FIGURE 6 Example of concurrent behavior of anomalies in MODIS spatial data products.

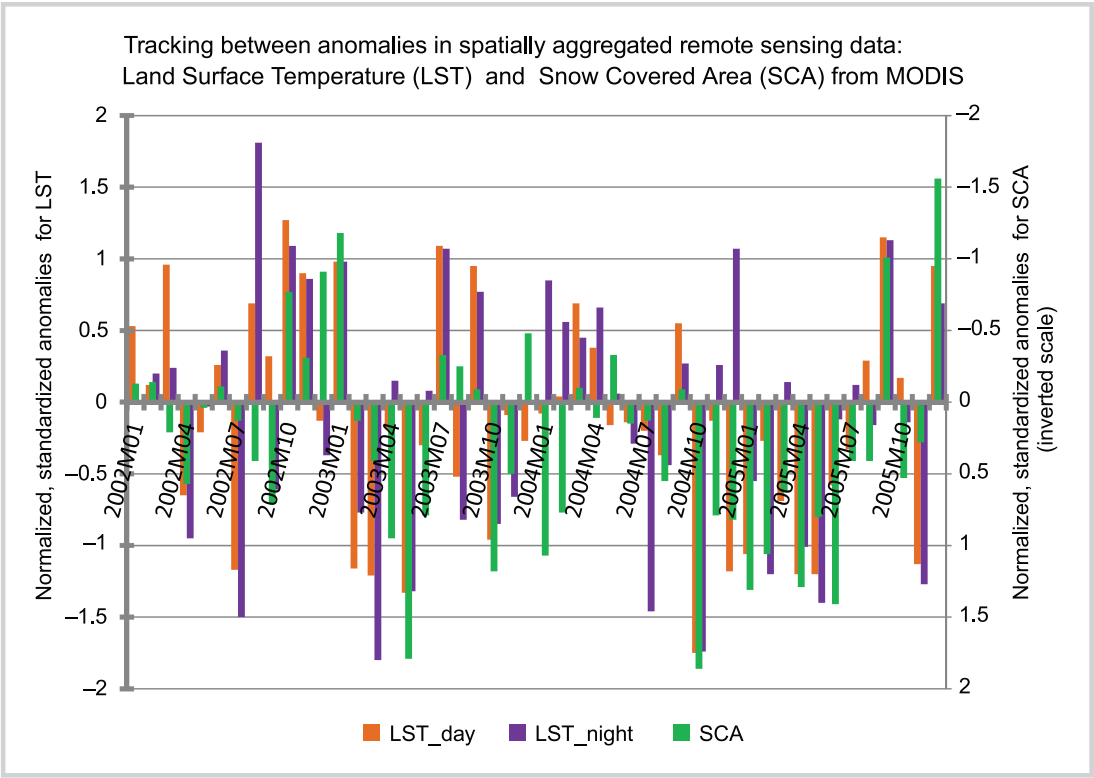

with climatic perturbations is the accurate assessment of the likely climatic variability (Wilby and Dessai 2010). An initial step in this assessment is quantification of present variability. Figure 7A, B depicts the annual cycles (period mean) and observed interannual variability (estimated 10th [c10] and 90th [c90] percentiles) of SCA and LST-derived continuous melt area, respectively, from the MODIS record for the large gauged tributaries of the UIB. As shown in "Large-scale hydrology of the UIB" above, variability in runoff from these tributaries is known to track locally observed variation in mass (precipitation) and energy (continuous melt area) inputs. As shown in this section, SCA and LST can provide viable spatial analogues for these local observations.

The differences between catchments in the shape of their annual SCA cycles, as shown in Figure 7A, align with established hydrological regime types. The catchments with high annual minima, Hunza and Shigar, are also those with high glacial melt contributions and minimal hydrological responsiveness to year-to-year variation in observed precipitation. Those with low annual minima, Gilgit and Astore, are snowmelt-dominated catchments dependent on annual replenishment of the snowpack from winter precipitation. Snowmelt regime catchments tend to have very little contributing area above 6000 m above sea level (masl). The relative variability in annual SCA minima (values for c10 compared to c90) is striking, particularly for the snowmelt-type catchments, Astore and Gilgit, where c90 is roughly twice c10 for the minimum month.

For water resources management purposes, either extreme in annual minima, c10 or c90, could indicate resource stress conditions. An extremely low annual minimum could indicate low preceding snowpack input (snowfall drought) and thus low catchment yield. Alternatively, a high annual minimum could indicate inadequate melt energy (cold summer) and thus inadequate ablation. Clearly the annual SCA minimum alone is an incomplete indicator. At the opposite end of the melt season, however, a lower than normal annual SCA maximum (in February or March) could provide an early warning of summer water shortfalls, giving local stakeholders time to prepare and enact contingency plans.

As for SCA, differences in the shape of annual cycles of CMA, as shown in Figure 7B, are indicative of differing hydrological regime types. While for snowmelt-type catchments (Gilgit and Astore) annual SCA minima showed the greatest relative variability, for glacial melt catchments (Hunza and Shigar) the relative variability annual maximum CMA is the key parameter in interannual climate variability. These glacial catchments have a low mean annual CMA maximum but a large relative variability (ratio of c90 to c10). Snowmelt-type catchments, in contrast, regularly attain very high CMA maxima because little of their area remains melt-free

http://dx.doi.org/10.1659/MRD-JOURNAL-D-11-00027.1

FIGURE 7 (A) Annual SCA cycle and interannual variability in major gauged tributary basins from MODIS data; (B) annual continuous melt area cycle and interannual variability in major gauged tributary basins. 0, NW UIB; 1, Hunza river to Dainyor bridge; 2, Shigar river to Shigar town; 3, Gilgit river to Gilgit town; 4, Astore river to Doyian; X, Upper Indus to Besham. (This figure also appears in Forsythe et al 2011, as their Figures 13 and 15.)

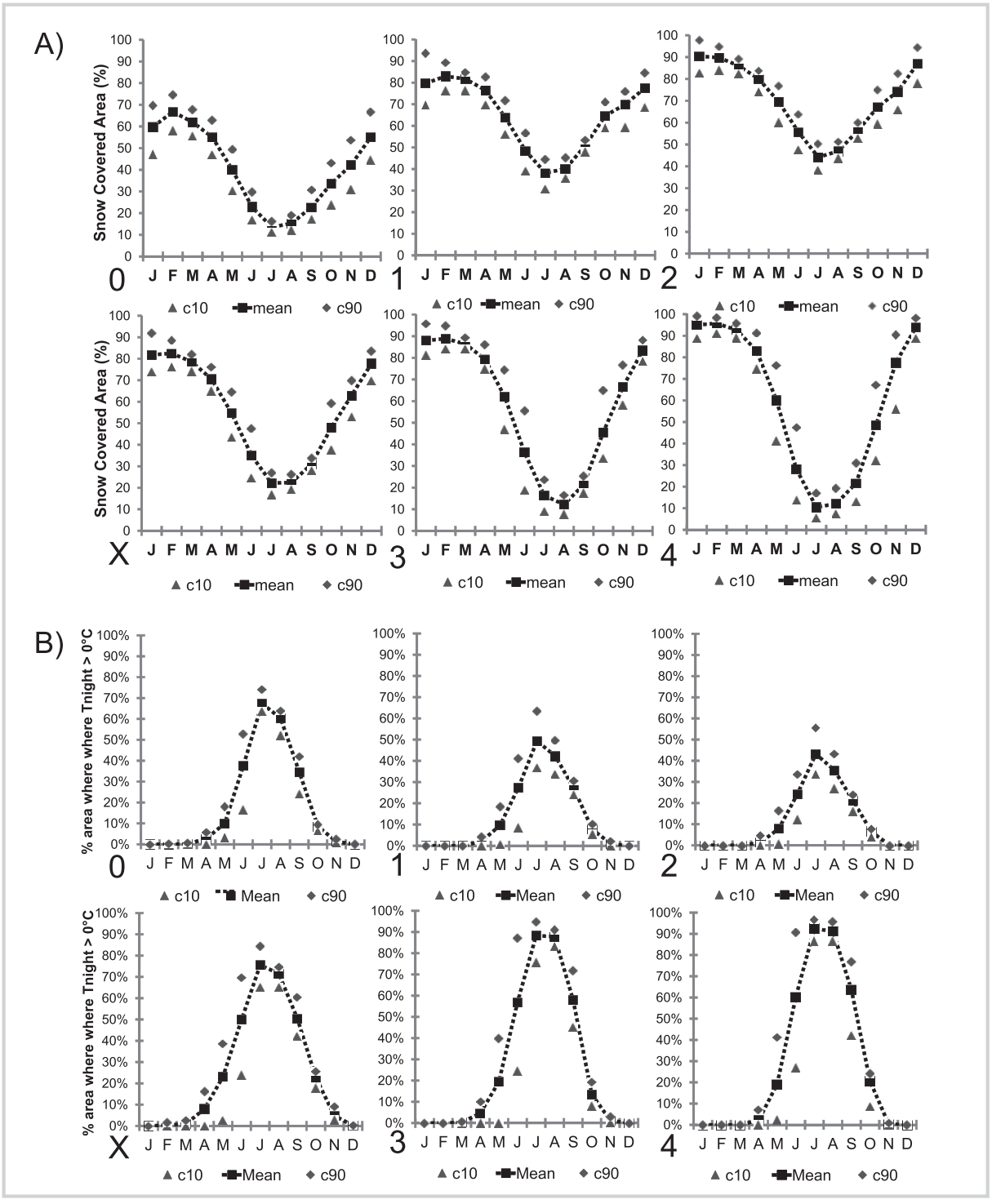

during the high summer. Another interesting element from Figure 7B is the consistency of the very large ranges in CMA during the early stages of the ablation phase (May and June); this can affect the timing of peak flows for both regime types as well as the availability of meltwater for irrigation during crucial crop growth phases. Some of this variability could be a result of apparent seasonal low-elevation nighttime LST inversions found when studying

http://dx.doi.org/10.1659/MRD-JOURNAL-D-11-00027.1

TABLE 1 Linear rate (°C/y) statistical measures for trends in daily minimum temperature for 3 stations in the UIB.[a)]

Station	Parameter	Mean daily minimum temperature (Tmin)					Mean daily maximum temperature (Tmax)				
	Season	Annual mean	DJF	MAM	JJA	SON	Annual mean	DJF	MAM	JJA	SON
Gilgit	Linear rate	**−0.033**	0.000	−0.016	**−0.063**	**−0.052**	**0.034**	**0.048**	**0.053**	−0.001	**0.040**
	Correlation measure	***−0.534***	−0.010	−0.293	***−0.606***	***−0.566***	***0.569***	***0.562***	0.477	−0.020	***0.526***
	P value	***0.001***	0.948	**0.049**	***0.001***	***0.001***	***0.001***	***0.001***	***0.001***	0.896	***0.001***
Skardu	Linear rate	−0.013	**0.024**	−0.006	**−0.032**	**−0.025**	**0.054**	**0.065**	**0.068**	**0.021**	**0.073**
	Correlation measure	−0.245	0.197	−0.112	−0.409	−0.377	***0.639***	0.462	***0.581***	0.218	***0.702***
	P value	0.101	0.190	0.459	***0.005***	**0.010**	***0.001***	***0.002***	***0.001***	0.146	***0.001***
Astore	Linear rate	0.008	0.019	**0.028**	−0.019	0.006	0.017	**0.021**	**0.030**	−0.009	**0.030**
	Correlation measure	0.180	0.196	0.407	−0.261	0.138	0.315	0.238	0.270	−0.122	0.422
	P value	0.232	0.192	***0.005***	0.080	0.361	**0.033**	0.112	0.070	0.420	***0.004***

[a)]Linear trend rates are in **bold** if absolute value is >0.02 (2°C/century). **Positive rates (warming)** are in simple bold, while **negative rates (cooling)** are bold underlined. Rates are greyed out if absolute value is <0.002. Values for Pearson's "***r***" (correlation measure) are bold, italic, and underlined if ***absolute value greater than 0.5***, but greyed out if absolute value is <0.25. Values for statistical significance are bold, italic, and underlined for ***P values of <0.01***, simple bold for ***P values of <0.05***.

http://dx.doi.org/10.1659/MRD-JOURNAL-D-11-00027.1

TABLE 2 Nonparametric measures of trend detection for local observations in summer (JJA) Tmin and winter (ONDJFM) wet days.

Nonparametric tests for trend detection		Trend in summer (JJA) mean daily minimum temperature (Tmin)				Trend in winter (ONDJFM) wet days (days with measured precipitation)			
		1962 to 2007		2000 to 2007		1959 to 2009		2000 to 2009	
Station	Test	Spearman	Kendall	Spearman	Kendall	Spearman	Kendall	Spearman	Kendall
Gilgit	Correlation measure	***−0.639***	**−0.450**	***0.611***	**0.400**	**0.380**	0.259	0.177	0.092
	P value	***0.0000***	***0.0000***	0.1077	0.2124	***0.0059***	***0.0088***	0.6240	0.7859
Skardu	Correlation measure	**−0.393**	−0.250	***−0.762***	***−0.571***	0.144	0.092	0.188	0.111
	P value	**0.0068**	**0.0153**	**0.0368**	0.0635	0.3129	0.3536	0.6076	0.7205
Astore	Correlation measure	−0.284	−0.182	−0.048	−0.071	**−0.308**	−0.207	−0.103	−0.111
	P value	0.0562	0.0794	0.9349	0.9015	**0.0277**	**0.0344**	0.7850	0.7205

the "parent data product" (MOD11A2). At present it is unclear whether this phenomenon is a real climatic feature of the UIB, perhaps linked to local-scale cloud cover variations, or an artifact resulting from a particular element in the algorithm.

Locally observed recent climate trends

The multidecadal life span of most water resources' infrastructure necessitates design not only for present climate variability but also for probable future conditions. A simple analysis of annual mean temperature change is inadequate to capture key hydrological processes, especially in meltwater-type regimes. Determining the direction and rate of year-on-year change throughout the annual cycle is essential in assessing probable future water resource availability (Rees and Collins 2005). Fowler and Archer (2006) analyzed the available records of 6 UIB meteorological stations for the period 1961 to 1999. While they identified a general upward trend of 0.007°C in annual mean temperatures, similar to the global trend over the same period, notable differences appeared when the contributions from individual seasons and the diurnal components (Tmax and Tmin) were separated. Specifically, they detected not only rising winter temperatures, primarily Tmax, but also cooling summer temperatures, especially summer Tmin. These asymmetrical trends in Tmax and Tmin thus yield an increase in diurnal temperature range (DTR) in all seasons. This contradicts general global patterns whereby faster increases in Tmin than Tmax yield decreasing DTR (Karl et al 1993; Easterling et al 1997). The present analysis updates the ground-based assessment to 2007 for 3 key stations.

Table 1 shows the estimated linear trends rates based on observations from the updated period (1962 to 2007) for the selected stations (Gilgit, Skardu, and Astore). Table 1 shows that the trend sign and magnitude, for either Tmin or Tmax, for each station generally agree with the others. The updated analysis supports the previous findings of substantial interseasonal asymmetry, as for most seasons and stations trends in Tmax and Tmin have opposite signs and contrasting rates. Tmax is observed to be rising quickly in winter (DJF), spring (MAM), and autumn (SON) but shows little if any change in summer (JJA). Indeed Tmin, by contrast, is decreasing rapidly in summer (JJA) with some decreases also in autumn (SON). In winter (DJF), weak increases or no changes in Tmin are observed. Thus, this analysis shows the increasing trend in DTR found by Fowler and Archer (2006) to be continuing throughout the annual cycle. DTR increases have also been reported for parts of India (Kumar et al 1994).

Nonparametric trend assessment

While linear estimation of observed change is a familiar and easily conceptualized measure of nonstationary

http://dx.doi.org/10.1659/MRD-JOURNAL-D-11-00027.1

TABLE 3 Nonparametric measures of trend detection for spatial data: summer (JJA) CMA and March SCA.

Nonparametric tests for trend detection		Trend in summer (JJA) continuous melt area (CMA)		Trend in March SCA	
		2000 to 2009		2000 to 2010	
Station	Test	Spearman	Kendall	Spearman	Kendall
Indus to Besham [X]	Correlation measure	−0.079	−0.111	0.045	−0.055
	P value	0.8380	0.7205	0.9030	0.8763
NW UIB [0]	Correlation measure	−0.273	−0.156	0.273	0.164
	P value	0.4483	0.5915	0.4182	0.5334
Hunza to Dainyor [1]	Correlation measure	−0.236	−0.111	0.264	0.200
	P value	0.5139	0.7205	0.4345	0.4363
Shigar to Shigar [2]	Correlation measure	−0.091	−0.067	0.264	0.147
	P value	0.8114	0.8580	0.4324	0.58465
Gilgit to Gilgit [3]	Correlation measure	−0.292	−0.270	0.320	0.241
	P value	0.4133	0.3232	0.338	0.34726
Astore to Doyian [4]	Correlation measure	−0.285	−0.200	0.045	0.055
	P value	0.4274	0.4743	0.9030	0.8762

systems, other methods of trend assessment that are less sensitive to outliers and less dependent on record length for test performance are available. Two popular methods are the "rank Spearman" and "Mann-Kendall" tests. These tests have been previously applied by Shrestha et al (1999) to assess temperature trends across Nepal by physiographic region.

While the Spearman and Mann-Kendall methods are statistically robust, they are still subject to the underlying climatic behavior of the chosen periods. A well-publicized example would be to considered global temperatures across a range of time periods; for example, 1961 to 2010 or 1998 to 2010. The underlying physical drivers of temperature change do not vary between the 2 time windows, but owing to the large range of underlying interannual variability, the magnitude and even signs of the estimated trend can be affected by what is otherwise an arbitrary choice of analysis window. To illustrate this with specific reference to the UIB, Table 2 presents the Spearman (rho) and Mann-Kendall (tau) measures of correlations of the observed series to time. Both Spearman's rho and Mann-Kendall's tau have the same bounds: −1 to +1. Respective estimates of statistical significance (*P* value) are also given. Two analysis windows are presented for each parameter: (1) summer (JJA) Tmin and (2) winter (ONDJFM) wet days. The longer analysis window corresponds to the entire available record length. The shorter window corresponds to part of the record overlapping with the MODIS record.

The signs, magnitudes, and *P* values from the Spearman and Mann-Kendall tests agree well within each parameter–window pairing. The magnitude, *P* value, and even sign can change dramatically between the analysis windows, however. The most striking example here is the opposite sign but equivalent magnitude for Tmin at Gilgit when switching from long window (1962 to 2007) to short window (2000 to 2007). The weaker (larger) *P* values for the shorter analysis windows are a function primarily of the shorter record length but also of the considerable interannual variability during the past decade. The UIB is similar to many regions globally in this regard. This variability should be borne in mind when considering the results of the Spearman and Mann-Kendall tests for the spatial data products as shown in Table 3.

It could be tempting to overinterpret the results presented in Table 3, to note consistent if weak negative correlation measures across the catchments for summer CMA and similarly consistent if weak positive values for March SCA. Objective consideration of the reported *P* values, however, inescapably points to the absence of

http://dx.doi.org/10.1659/MRD-JOURNAL-D-11-00027.1

TABLE 4 Potential impacts for the Hunza catchment from summer (JJA) minimum/nighttime temperature change.

Summer (JJA) mean temperature change (°C)	Isotherm elevation change (m)	Tnight from MODIS LST				Tmin from 2 m air temperature (PMD)			
		0 °C isotherm elevation (m)	CMA (%)	CMA change (%)	Relative runoff change (%)	0 °C isotherm elevation (m)	CMA (%)	CMA change (%)	Relative runoff change (%)
−4.0	−620	4000	27.4	−22.0	−30.3	4300	37.4	−26.1	−36.0
−2.0	−310	4300	37.4	−12.0	−16.5	4600	49.4	−14.1	−19.4
−0.75	−110	4500	45.1	−4.3	−5.9	4800	58.9	−4.6	−6.3
0	0	4600	49.4	0.0	0.0	4900	63.5	0.0	0.0
+0.75	110	4700	54.0	4.6	6.3	5000	68.4	4.9	6.7
+2.0	310	4900	63.5	14.1	19.4	5200	78.2	14.7	20.3
+4.0	620	5200	78.2	28.8	39.7	5500	89.5	26.0	35.9

strong, statistically significant trends. The latter finding is in fact the important element—ie whatever spatially distributed changes are under way, it will take time before trends clearly emerge from the ambient noise of interannual variability.

Results and discussion

In the study of the UIB, spatial climate data derived from satellite imagery and point measurements from local weather stations are complementary tools for understanding the drivers of a complex and dynamic hydrological system. Spatial data products provide key insights into patterns linked to steep topographic gradients. Long-record data series provided by a network of local weather stations permit quantitative assessment of regional patterns of variability and change. Previous studies have established that predictive relationships exist between meteorological point observations and discharge in the large gauged tributary basins of the UIB. Forsythe et al (2011) demonstrated that remotely sensed spatial data products (MODIS SCA and LST) can provide adequate analogues for these point observations. Used together, the 2 types of data may improve assessments of the likely hydrological impacts of projected climate change. These impacts may well vary between UIB subcatchments based on their hydrological regime type (eg perennial ice or seasonal snow). Examination of the variability only in the record of the available data products (early 2000 to present) indicates considerable potential hydrological variability in key seasons for water resources management.

In catchments such as the Hunza, where glacial melt provides a significant contribution to runoff, summer ablation season energy inputs—indexed by temperature—govern runoff volumes (Archer 2003). Specifically, these catchments appear to be sensitive to Tmin. Observations from ground-based measurements seem to indicate a strong decreasing trend in summer Tmin. Propagation of this trend from valley stations upward through the catchment is thus of particular concern, as it may greatly inhibit summer runoff generation. Projections from the Intergovernmental Panel on Climate Change (Solomon et al 2007), however, suggest increasing temperatures in the UIB in all seasons over the next century. Thus, it is not yet clear whether the recent local summer (JJA) Tmin observations simply show a transitory phenomenon as the climate seeks a new equilibrium state or if they are evidence of a regional divergence from the global pattern due to realignment of large-scale circulation or relative changes in components of the local energy balance.

Given this uncertainty, it is prudent to examine the potential consequences from a range of potential temperature changes. These consequences are quantified in Table 4. The isotherm elevation changes are based on a lapse rate of 0.0064°C/m. The potential changes in relative

http://dx.doi.org/10.1659/MRD-JOURNAL-D-11-00027.1

runoff volume for the Hunza catchment are calculated using the coefficient (1.3816) shown in Figure 3D. As can be seen in Table 4, even moderate temperature change ($\pm 2^{\circ}$C) could result in changes of $\pm 20\%$ in mean summer runoff. It is important to understand that these shifts in isotherm elevation would also have important impacts on glacial dynamics in the UIB by shifting the equilibrium line altitude (ELA) and thus the accumulation area ratio (AAR).

In light of the discrepancy between recently locally observed trends and projected future change, it would be extremely valuable to corroborate the local ground-based measurements with long-record spatial data products. To this end, parallel work is currently under way on development of multidecadal spatial data products—equivalent to MODIS SCA and LST—using imagery from the Advanced Very High Resolution Radiometer (AVHRR) instrument flown on several generations of U.S. National Oceanic and Atmospheric Agency (NOAA) satellites (Chokmani et al 2005, Khlopenkov and Trischenko 2006, Li and Becker 1993, Pinheiro et al 2006). At present AVHRR sensor data covering the MODIS record have been acquired and processed using the initial versions of the algorithms adapted from the methodologies of the authors cited. The validation process will thus include comparison with the two equivalent MODIS data products as well as evaluation against local observations using the analysis approach presented here.

If successful, construction of a multidecadal spatial record of SCA and LST would allow both direct estimation of recent trends and assessment of relationships between these regional patterns and larger-scale atmospheric phenomena. Long-record LST analyses aim to assess the multidecade evolution of 0°C isotherm elevations and thus the distribution of solid (snowfall) versus liquid (rainfall) precipitation. Long-record SCA data will be assessed as depletion versus available discharge. Extending the record of spatial data backward in time would be especially useful because this would greatly increase the overlap with available river gauging data. Combinations of scenarios within the observed record that are judged likely to become more frequent in the future may then be used as analogues for future hydrological conditions.

ACKNOWLEDGMENTS

Nathan Forsythe was supported by a Graduate Research Fellowship award from the U.S. National Science Foundation as well as by project-based support from the British Council and the School of Civil Engineering & Geosciences of Newcastle University. Hayley Fowler was supported by NERC Postdoctoral Fellowship award NE/D009588/1 (2006–2010). Funds for travel between the UK and Pakistan and for capacity building activities were provided by the British Council through its PMI2Connect and INSPIRE research exchange award programs. We wish to thank the Pakistan Meteorological Department and the Water and Power Development Authority for the provision of climate and flow data.

REFERENCES

Archer DR. 2003. Contrasting hydrological regimes in the upper Indus Basin. *Journal of Hydrology* 274(1–4):198–210.

Archer DR, Forsythe N, Fowler HJ, Shah SM. 2010. Sustainability of water resources management in the Indus Basin under changing climatic and socio economic conditions. *Hydrology and Earth System Sciences* 14:1669–1680. http://dx.doi.org/10.5194/hess-14-1669-2010.

Archer DR, Fowler HJ. 2008. Using meteorological data to forecast seasonal runoff on the River Jhelum, Pakistan. *Journal of Hydrology* 361(1–2):10–23.

Bengtsson L. 1982. The importance of refreezing on the diurnal snowmelt cycle with application to a Northern Swedish catchment. *Nordic Hydrology* 13: 1–12.

Bras RL. 1990. Chapter 6: Snowpack and snowmelt. *In:* Bras RL, editor. *Hydrology: An Introduction to Hydrologic Science.* Reading, MA: Addison-Wesley, pp 247–281.

Chokmani K, Bernier M, Slivitzky M. 2005. Suivi spatio-temporel du couvert nival du Québec à l'aide des données NOAA-AVHRR. *Revue des sciences de l'eau/Journal of Water Science* 1(3):163–179. http://id.erudit.org/iderudit/013536ar.

Dinku T, Chidzambwa S, Ceccato P, Connor SJ, Ropelewski CF. 2008. Validation of high resolution satellite rainfall products over complex terrain. *International Journal of Remote Sensing* 29(14):4097–4110. http://dx.doi.org/10.1080/01431160701772526.

Easterling DR, Horton B, Jones PD, Peterson TC, Karl TR, Parker DE, Salinger MJ, Razuvayev V, Plummer N, Jamason P, Folland CK. 1997. Maximum and minimum temperature trends for the globe. *Science* 277:364–367.

Forsythe N, Fowler HJ, Kilsby CG, Archer DR. 2011. Opportunities from remote sensing for supporting water resources management in village/valley scale catchments in the Upper Indus Basin. *Water Resources Management* Online first. http://dx.doi.org/10.1007/s11269-011-9933-8.

Fowler HJ, Archer DR. 2006. Conflicting signals of climatic change in the upper Indus Basin. *Journal of Climate* 19(17):4276–4293.

Hall DK, Riggs GA, Salomonson VV, Barton JS, Casey K, Chien JYL, DiGirolamo NE, Klein AG, Powell HW, Tait AB. 2001. Algorithm Theoretical Basis Document (ATBD) for the MODIS snow and sea ice-mapping algorithms. http://modis-snow-ice.gsfc.nasa.gov/atbd01.html; accessed in October 2011.

Hewitt K. 2011. Glacier change, concentration, and elevation effects in the Karakoram Himalaya, Upper Indus Basin. *Mountain Research and Development* 31(3):188–200.

Huffman GJ, Adler RF, Bolvin DT, Gu G, Nelkin EJ, Bowman KP, Hong Y, Stocker EF, Wolff DB. 2007. The TRMM Multisatellite Precipitation Analysis (TMPA): Quasi-global, multiyear, combined-sensor precipitation estimates at fine scales. *Journal of Hydrometeorology* 8:38–54. http://dx.doi.org/10.1175/JHM560.1.

Immerzeel WW, Beek LPHv, Bierkens MFP. 2010. Climate change will affect the Asian water towers. *Science* 328:1382–1385.

Jain SK, Goswami A, Saraf AK. 2008. Accuracy assessment of MODIS, NOAA and IRS data in snow cover mapping under Himalayan conditions. *International Journal of Remote Sensing* 29(20):5863–5878. http://dx.doi.org/10.1080/01431160801908129.

Karki MB, Shrestha AB, Winiger M. 2011. Enhancing knowledge management and adaptation capacity for integrated management of water resources in the Indus River Basin. *Mountain Research and Development* 31(3):242–251.

Karl TR, Jones PD, Knight RW, Kukla G, Plummer N, Razuvayev V, Gallo KP, Lindseay J, Charlson RJ, Peterson TC. 1993. A new perspective on recent global warming—asymmetric trends of daily maximum and minimum temperature. *Bulletin of the American Meteorological Society* 74:1007–1023.

Khlopenkov KV, Trishchenko AP. 2006. SPARC: New cloud, snow, and cloud shadow detection scheme for historical 1-km AVHHR data over Canada. *Journal of Atmospheric and Oceanic Technology* 2(3):322–343. http://dx.doi.org/10.1175/jtech1987.1.

Kumar KR, Kumar KK, Pant GB. 1994. Diurnal asymmetry of surface temperature trends over India. *Geophysical Research Letters* 21:677–680.

Li ZL, Becker F. 1993 Feasibility of land surface temperature and emissivity determination from AVHRR data. *Remote Sensing of Environment* 43:67–85.

Pinheiro ACT, Mahoney R, Privette JL, Tucker CJ. 2006. Development of a daily long term record of NOAA-14 AVHRR land surface temperature over Africa. *Remote Sensing of Environment* 103:153–164. http://dx.doi.org/10.1016/j.rse.2006.03.009.
Rees HG, Collins DN. 2005. Regional differences in response of flow in glacier-fed Himalayan rivers to climatic warming. *Hydrological Processes* 20(10):2157–2169.
Shrestha AB, Wake C, Mayewski PA, Dibb JE. 1999. Maximum temperature trends in the Himalaya and its vicinity: An analysis based on temperature records from Nepal for the period 1971–1994. *Journal of Climate* 12:2775–2786.
Solomon S, Qin D, Manning M, Chen Z, Marquis M, Averyt KB, Tignor M, Miller HL, editors. 2007. *Climate Change 2007: The Physical Science Basis*. Contribution of Working Group I to the Fourth Assessment Report of the Intergovernmental Panel on Climate Change. Cambridge, United Kingdom, and New York, NY: Cambridge University Press.
Wan Z. 2008. New refinements and validation of the MODIS land-surface temperature/emissivity products. *Remote Sensing of Environment* 112:59–74. http://dx.doi.org/10.1016/j.rse.2006.06.026.
Wilby RL, Dessai S. 2010. Robust adaptation to climate change. *Weather* 65(7):180–185. http://dx.doi.org/10.1002/wea.543.

Supplemental data

TABLE S1 Correlations of March snow covered area (SCA) versus cumulative winter (October–March) precipitation and wet days. (This table also appears in Forsythe et al 2011, as the first 7 rows of their Table 3.)
TABLE S2 Correlations of land surface temperature (LST) versus 2-m air temperature (point observations). (This table also appears in Forsythe et al 2011, as the first 7 rows of their Table 4.)
TABLE S3 Correlation between spatial variables within individual subcatchment. (This table also appears in Forsythe et al 2011, as their Table 5.)

Found at DOI: 10.1659/MRD-JOURNAL-D-11-00027.S1 (30 KB PDF).